AIMS Mathematics, 10(11): 27129–27151.
DOI: 10.3934/math.20251192
Received: 23 September 2025
Revised: 29 October 2025
Accepted: 04 November 2025
Published: 21 November 2025

https://www.aimspress.com/journal/Math

Research article

AI-driven analysis of Darcy-Forchheimer EMHD boundary layer flow in thermal hybrid nanofluids

Abdulaziz H. Alharbi[1,*], El Hadi Boussaha[2], Ali M. Alhartomi[3], Hicham Salhi[4], Raed Alrdadi[1], Mohamed Kezzar[5] and Mohamed Rafik Sari[6]

[1] Department of Mathematics, Jamoum University College, Umm Al-Qura University, Makkah 25375, Saudi Arabia
[2] Department of Process Engineering, Faculty of Technology, Universit´e 20 Aout 1955, ElHadaik Road, Skikda 21000, Algeria
[3] Department of Mathematics, Al-Leith University College, Umm Al-Qura University, Makkah 24382, Saudi Arabia
[4] Laboratory of Applied Research in Hydraulics, University of Mustapha Ben Boulaid, Batna2, Batna 05000, Algeria
[5] Materials and Energy Engineering Laboratory (LMGE), Technology Department, Faculty of Technology, 20 Aout 1955 University of Skikda, P. O. Box 26, 21000, Skikda, Algeria
[6] Mechanics of Materials and Plant Maintenance Research Laboratory (LR3MI), Mechanical Engineering Department, Faculty of Technology, Badji Mokhtar-Annaba University, P. O. Box 12, Annaba 23000, Algeria

* **Correspondence:** Email: ahhrbe@uqu.edu.sa.

Abstract: This study thoroughly examined the complex electro-magnetohydrodynamic (EMHD) boundary layer flow of ternary hybrid nanofluids (THNP), specifically, Ti6Al4V-ZnO-Fe_2O_3, over stretching-shrinking and permeable surfaces, and recognized the important impact of the nonlinear Darcy-Forchheimer law and thermal radiation. The THNP, comprised of three distinct nanoparticles including: titanium alloy Ti6Al4V (6% aluminum, 4% vanadium, balance titanium), zinc oxide ZnO, and iron oxide Fe_2O_3 suspended in a base fluid, is used to enhance both thermal and flow properties. The model comprehensively addressed inertial effects in porous media through the Darcy-Forchheimer drag, as well as the electromagnetic forces and thermal radiation. The governing partial differential equations were transformed into nonlinear ordinary differential equations via similarity transformations, which were solved through an intelligent numerical approach using artificial neural

networks (ANN). A thorough analysis was conducted on the effect of important parameters such as the Darcy-Forchheimer permeability, nanoparticle volume fractions, stretching/shrinking rates, surface permeability, and radiation intensity on the velocity and temperature profiles. The results are shown graphically and discussed, providing insight related to the fluid dynamics and heat-transfer phenomena in such advanced systems.

Keywords: artificial intelligence; artificial neural networks; Darcy-Forchheimer law; THNP; EMHD; stretching/shrinking; intelligent numerical approach
Mathematics Subject Classification: 35A22, 76A05, 76D05, 76S05, 76W05

1 Introduction

For almost a century, the study of boundary layer flows over many geometries has been a crucial element of fluid mechanics research. It has been applied to fields such as aerospace engineering and biomedical devices. Recently, a large number of research works have explored various boundary layer flow problems. Notable research work on boundary layer flow include those by Abbasbandy et al. [1], Hayat et al. [2], Eid and Mahny [3], and Gherieb et al. [4]. The study conducted by Liaqat et al. [5] assessed the transient rotating three-dimensional boundary layer flow of micropolar fluid induced by the Riga plate. In another researchwork, Liaqat et al. [6] investigated the impact of entropy generation on the thermal transport and momentum of a continuous two-dimensional dusty fluid magnetohydrodynamic (MHD) migration across an inclined stretched sheet.

In the past few years, the integration of electromagnetic effects and nanofluid suspensions has accelerated advancements in heat and mass transfer, particularly pertinent to contemporary industrial applications that include magnetic drug targeting, electromagnetic flow regulation, and sophisticated heat exchangers [7–9]. The Darcy-Forchheimer law has been adopted to examine fluid dynamics within a porous object and becomes significant in boundary layer study due to its capacity to merge viscous and inertial forces in fluid dynamics. The linear connection between the pressure gradient and velocity could be discribed by Darcy's law and the Darcy-Forchheimer law added the important term, which is to integrate a quadratic velocity when increasing Reynolds mbers [10–12]. Liaqat et al. [13] investigated the problem of steady two-dimensional magnetohydrodynamics (MHD) migration of dusty fluid across a stretching sheet with the inclusion of Darcy-Forchheimer porosity and Brownian dispersion. The nonlinear behavior is important in electromagnetic applications; for example, Lorentz forces can generate intricate flow patterns and velocity profiles. Electromagnetohydrodynamic (EMHD) flows show a significant convergence of fluid mechanics and electromagnetic theory, where electric and magnetic fields could affect the motion of fluid. The system of governing equations for EMHD flows includes extra body forces resulting from the interaction between induced currents as well as applied electromagnetic fields. This changes the equations for momentum and energy [14,15]. These flows are commonly used in microfluidic devices, plasma physics, and materials processing fields where precise control of fluid motion is important. The further development of ternary hybrid nanofluids (THNF) implies the most recent development in nanofluid technology. Traditional nanofluids usually employ single-type nanoparticles, while ternary hybrid systems mix three different types of nanoparticles inside a base fluid to provide synergistic enhancements in thermal conductivity, viscosity, and other transport properties [16,17]. The thermal conductivity of optimally formulated THNF compositions could increase by as much as 13.3% compared to traditional nanofluid, according

to the last experimental research, while maintaining sufficient stability for heating and cooling applications [18,19]. Because EMHD boundary layer flows with THNF under Darcy-Forchheimer conditions are nonlinear partial differential equations, the analytic solution of this system is complicated, which means numerical techniques are required. The system of equations includes momentum, energy, and electromagnetic field equations, and thermal physical parameters depend on nanoparticle concentration and electromagnetic field strength [13,14,20,21]. Wakif et al. [22] studied theoretically the convectively heated nanofluid during its two-dimensional EMHD boundary layer flow in the laminar and steady states over a horizontal electromagnetic plate. They found that the nanofluid rapidity exhibits an increasing dynamical behavior and the skin friction coefficient shows a significant alteration for the nanoparticles' volume fraction and the porosity effect. The study done by Mushahary et al. [23] explored the mixed convective electro-osmotic and electro-magnetohydrodynamic (EMHD) flow of a coupled stress hybrid nanofluid through a porous vertical channel. This investigation shows the impacts of nanofluid nanoparticles, electro-osmosis, thermal radiation, an electromagnetic field, variable electrical conductivity, variable porous permeability, and thermal radiation on temperature and velocity profiles, entropy generation, and the shear stresses and heat transfer rates. Computational fluid dynamics methodologies, although precise, are resource-intensive and time-consuming for parametric analyses and optimization challenges. Artificial neural networks (ANNs) have been used for solving difficult fluid mechanics problems because they are much faster than traditional methods. The last investigation has employed ANNs to tackle the multi-boundary layer and showcased their capacity to identify nonlinear correlations and deliver swift resolutions for parametric fluctuations [24–26]. The theorem of universal approximation highlighted that well-designed neural networks can closely match any continuous function, which makes them great for investigating complicated multi-physics problems such as EMHD flows [27]. With the help of machine learning techniques, researchers have used different types of neural networks to predict heat transfer coefficients, friction factors, and temperature distributions in nanofluid flows [28,29]. In their interesting research, Zia et al. [29] simulated the EMHD Darcy-Forchheimer flow of Casson hybrid nanofluid over a stretching surface employing an innovative artificial neural networks (ANNs) based on the Levenberg-Marquardt backpropagation scheme. They explored the effects of electro-osmosis, Joule heating, and porous media interactions on Casson hybrid nanofluid under EMHD-DF flow conditions.

The particular combination of EMHD effects, the Darcy-Forchheimer flow regime, and ternary hybrid nanofluids introduces distinct challenges necessitating meticulous attention to network architecture, training data generation, and validation methodologies. Even though there has been a lot of progress in specific areas of EMHD flows, porous media effects, and nanofluid applications, there is still a big gap in our understanding of how they all work together to change the properties of the boundary layer. The combined effects of electromagnetic forces, porous media resistance, and ternary hybrid nanofluid properties on heat and mass transfer have not been thoroughly studied with modern machine learning methods. Also, for engineering to work in the real world, it is important to make prediction models for these kinds of complex systems that are easy to use with computers. The primary originality of this research is the development of an artificial-intelligence-based framework to comprehensively study and understand the Darcy-Forchheimer electromagnetic hydrodynamic (EMHD) boundary-layer flow and heat transference behavior of thermal hybrid nanofluids over a porous surface. Furthermore, the study focuses on investigating the influence of various physical parameters of interest like the magnetic parameter (M), electrical parameter (E), Prandtl number (Pr), radiation parameter (Rd), Eckert number (Ec), porosity parameter, and Darcy-Forchheimer parameter on the flow dynamics and thermal performances of a THNF-EMHD system. The investigation is

performed employing a combination of artificial neural networks (ANNs) and Runge-Kutta numerical schemes.

2 Basic model

The research investigates the behavior of an incompressible, two-dimensional THNF fluid over a flat surface, influenced by a vertically aligned electromagnetic field (comprising magnetic and electric fields), the Darcy-Forchheimer law, the radiation source and an opposing pressure gradient. Figure 1 illustrates the configuration of physical THNF-EMHD flow.

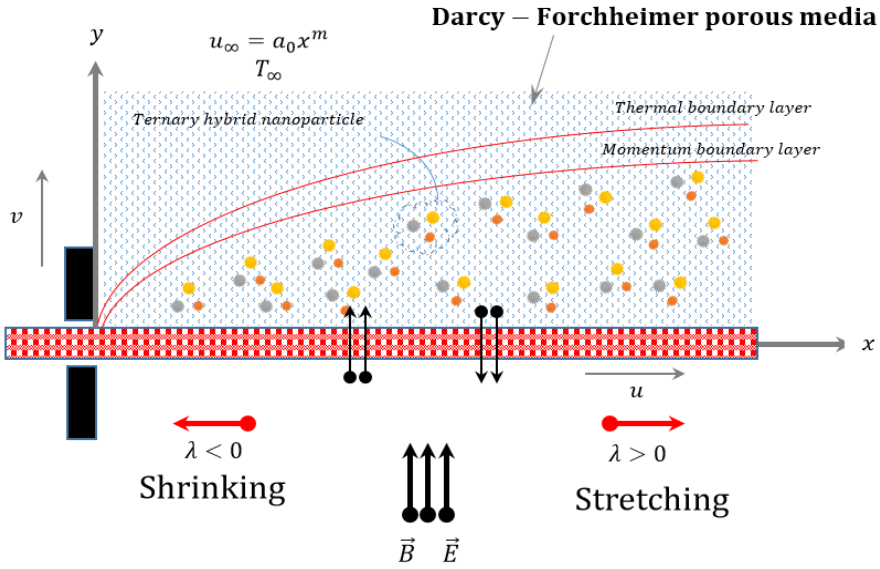

Figure 1. Configuration of THNF-EMHD flow.

The mass, momentum, and energy governing boundary layer equations for THNFs-EMHD flow are as follows:

$$\frac{\partial u}{\partial x} + \frac{\partial v}{\partial y} = 0. \tag{1}$$

$$u\frac{\partial u}{\partial x} + v\frac{\partial u}{\partial y} = u_\infty \frac{du_\infty}{dx} + \nu_{Thnf}\frac{\partial^2 u}{\partial y^2} + \frac{\sigma_{Thnf}}{\rho_{Thnf}}\left(E_0 B_0 - {B_0}^2 u + {B_0}^2 u_\infty\right) - \frac{\mu_{Thnf}}{\rho_{Thnf}\bar{K}}u - \frac{C_b}{\sqrt{\bar{K}}}u^2. \tag{2}$$

$$u\frac{\partial T}{\partial x} + v\frac{\partial T}{\partial y} = \alpha_{Thnf}\left(\frac{\partial^2 T}{\partial y^2}\right) - \frac{1}{(\rho C_p)_{Thnf}}\frac{\partial q_r}{\partial y} + \frac{1}{(\rho C_p)_{Thnf}}\sigma_{Thnf}(B_0 u - E_0)^2. \tag{3}$$

The boundary conditions are presented in Table 1:

Table 1. Boundary conditions.

	$x \to 0$	$x \to \infty$
Velocity profiles	$u(0) = u_w \; and \; v(0) = v_w$	$u(\infty) = u_\infty$
Temperature profiles	$T(0) = T_w$	$T(\infty) = T_\infty$

where

$$\begin{cases} u_\infty(x) = a_0 x^m \\ u_w = \lambda u_\infty \\ v_w = -\sqrt{\frac{u_\infty \nu_f}{2x}} \times S \end{cases}. \tag{4}$$

The Rosseland approximation for radiation is used to calculate the radiative heat flow q_r, and we obtain:

$$\frac{\partial q_r}{\partial y} \approx -\frac{16\sigma^* T_\infty^3}{3k^*}\left(\frac{\partial^2 T}{\partial y^2}\right). \tag{5}$$

We introduce the following similarity variables [31],

$$\left.\begin{aligned} \eta = \frac{y}{x}\sqrt{Re_x} = y\left(\frac{u_\infty}{\nu_f x}\right)^{1/2}, \\ \psi(x,y) = \left(u_\infty x \nu_f\right)^{1/2} f(\eta), \\ u = \frac{\partial \psi}{\partial y} = u_\infty f'(\eta), \\ v = -\frac{\partial \psi}{\partial x} = \frac{u_\infty}{\left(\frac{u_\infty x}{\nu_f}\right)^{1/2}}\left[\frac{(1-m)}{2}\eta f'(\eta) - \frac{(m+1)}{2} f(\eta)\right], \\ \theta = \frac{T - T_\infty}{T_w - T_\infty}. \end{aligned}\right\} \tag{6}$$

The following are the modified boundary conditions and governing equations:

$$f''' + A_1 A_2\left(m(1 - f'^2) + \frac{m+1}{2} f f''\right) - A_1 A_3 M(f' - \mathrm{E}_1 - 1) - \mathcal{K}_p f' - A_1 A_2 Frf'^2 = 0. \tag{7}$$

$$\left(1 + \frac{4}{3}\frac{Rd}{A_5}\right)\theta'' + \frac{A_4}{A_5} Pr\left(\frac{1}{2}(m+1) f\theta' - m f'\theta\right) + \frac{A_3}{A_5} PrMEc(f' - E_1)^2 = 0. \tag{8}$$

The boundary conditions of the problem are:

$$\begin{aligned} &\text{At } \eta \to 0\text{: } f(0) = \tau, \quad f'(0) = \lambda, \theta(0) = 1, \\ &\text{At } \eta \to \infty\text{: } f'(\infty) = 1, \quad \theta(\infty) = 0, \end{aligned} \tag{9}$$

where:

$\tau \to$ is permeability parameter,

$\lambda \to$ is stretching-shrinking parameter.

The following is a Descriptions of the physical quantities of importance in this study are presented in Table 2:

Table 2. The physical quantities.

Name	Expression
Magnetic parameter	$M = \frac{\sigma_f B_0^2}{\rho_f a_0}$
Electrical parameter	$E_1 = \frac{E_0}{B_0 u_\infty}$
Prandtl number	$Pr = \frac{\mu_f Cp_f}{k_f}$
Radiation parameter	$Rd = \frac{4T_\infty^3 \sigma^*}{k_f K^*}$
Eckert number	$Ec = \frac{u_\infty^2}{(Cp)_f \Delta T}$
Porosity parameter	$\mathcal{K}_p = \frac{\nu_f x}{U_\infty \widehat{K}}$
Darcy-Forchheimer parameter	$Fr = \frac{x C_b}{\sqrt{\widehat{K}}}$

And A_i, where $i = 1$ to 5, is taken as (see Appendix A):

$$\begin{aligned} A_1 &= (1-\phi_1)^{2.5}(1-\phi_2)^{2.5}(1-\phi_3)^{2.5}, \\ A_2 &= \frac{\rho_{Thnf}}{\rho_f}, \\ A_3 &= \frac{\sigma_{Thnf}}{\sigma_f}, \\ A_4 &= \frac{(\rho Cp)_{Thnf}}{(\rho Cp)_f}, \\ A_5 &= k_{Thnf}/k_f\,. \end{aligned} \tag{11}$$

The non-dimensional form of both the local Nusselt number $\langle Nu_x \rangle$ and the skin friction coefficient $\langle C_f \rangle$ at the plate $\langle \eta = 0 \rangle$ are written in Table 3.

Table 3. Engineering coefficients.

Skin friction coefficient $\langle C_f \rangle$	Local Nusselt number $\langle Nu_x \rangle$
$(Re_x)^{1/2} C_f = 2\frac{\mu_{Thnf}}{\mu_f} f''(0)$	$\frac{1}{(Re_x)^{1/2}} Nu_x = -\frac{k_{Thnf}}{k_f}\theta'(0)$

where Re_x is the local Reynolds number.

3 Methodology of ANNs

The network diagram (Figure 2) shows an artificial neural network (ANN) architecture for modeling the Role of the Darcy-Forchheimer law on EMHD boundary layer flow. It includes input layers with parameters like the magnetic and electrical fields, stretching/shrinking parameter, radiation source, porosity parameter, Darcy-Forchheimer parameter, hidden layers, and output layers. All of the figures are generated by systematically investigating a spectrum of values for a particular parameter,

such as: $m = 0.2, M = 0.2, \varphi_1 = \varphi_2 = \varphi_3 = 2\%, E1 = 0.2, R = 3, Kp = 0.2, \lambda = 0.2, \tau = 0.$

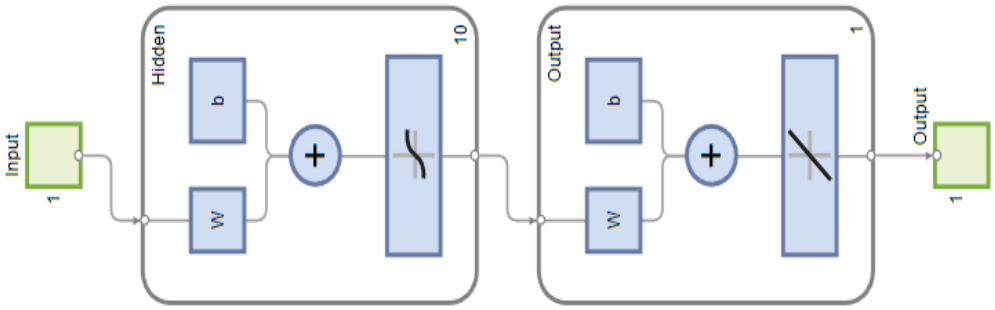

Figure 2. (a) Network diagram.

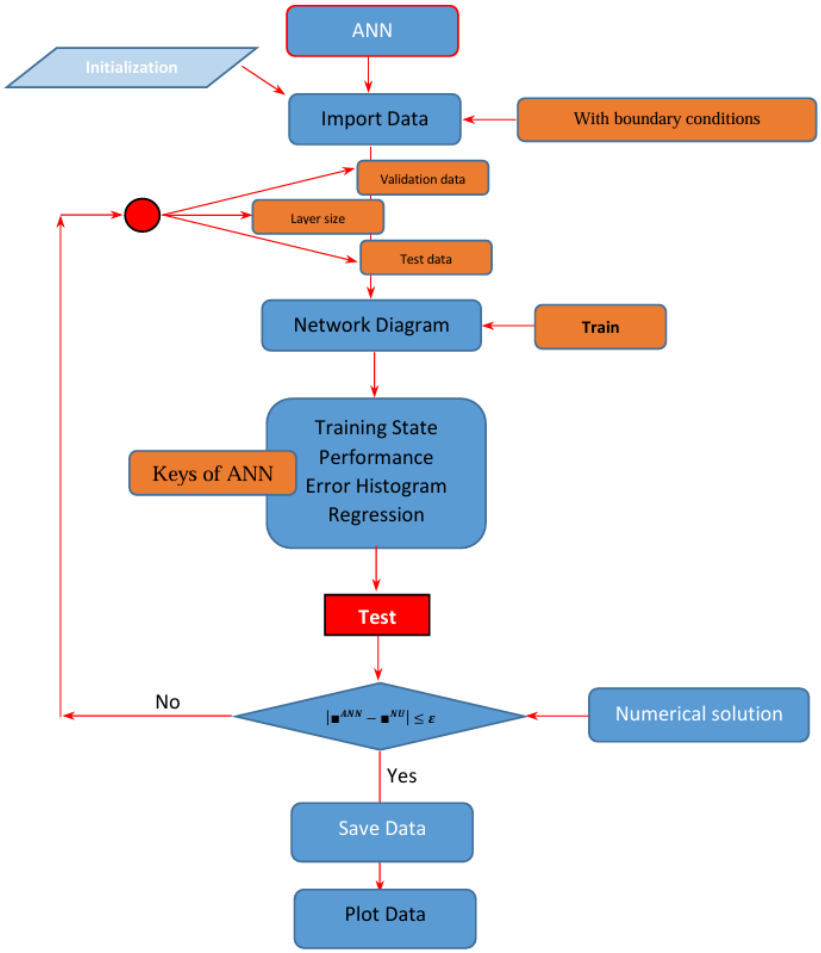

Figure 2. (b) ANN architecture.

The training process in Figure 3(a) was stable and effective, with no overfitting or instability. The network reached optimal weights and maintained good performance on the validation set. Figure 3(b) displays successful training of a neural network, achieving low errors, strong generalization, and no

overfitting, demonstrating a stable and effective training process. The neural network model exhibits accurate predictions, minimal bias, and strong generalization capability, as evidenced by the error histogram in Figure 3(c), clustered around zero for training, validation, and test sets. From Figure 3(d), results show that the points fall approximately on the straight line on the fitted models .In fact, the model provides better approximation for the velocity profile.

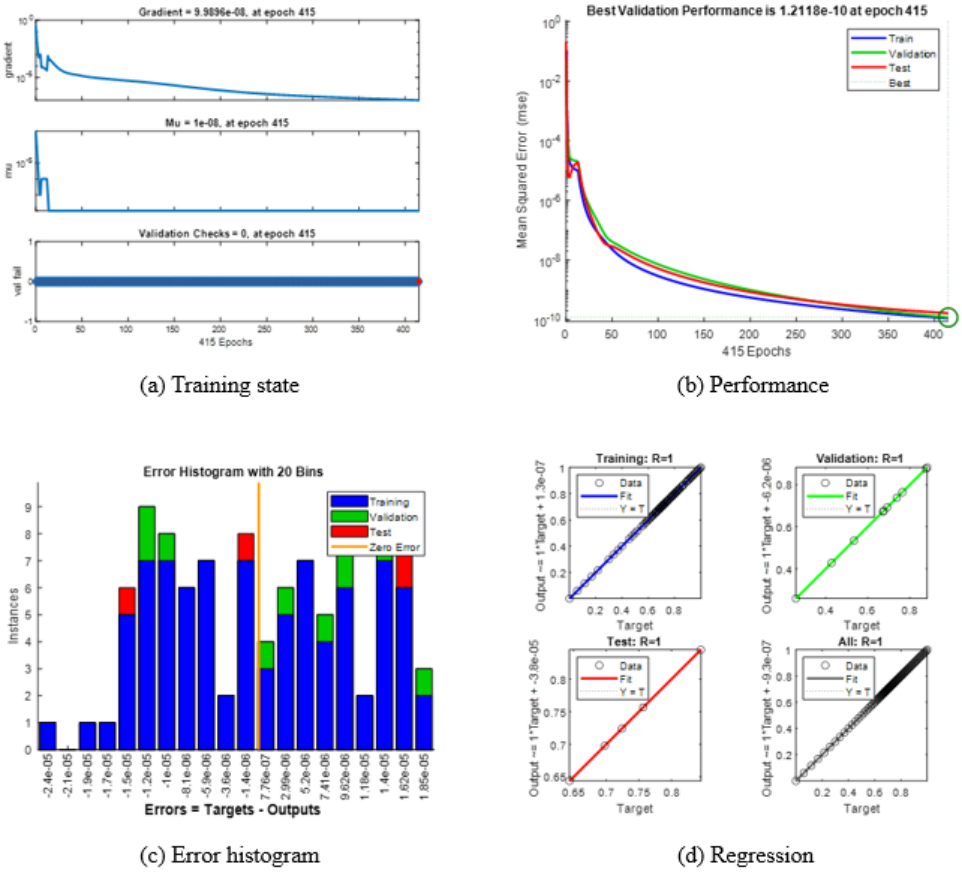

(a) Training state (b) Performance

(c) Error histogram (d) Regression

Figure 3. The key factors of $f'(\eta)$.

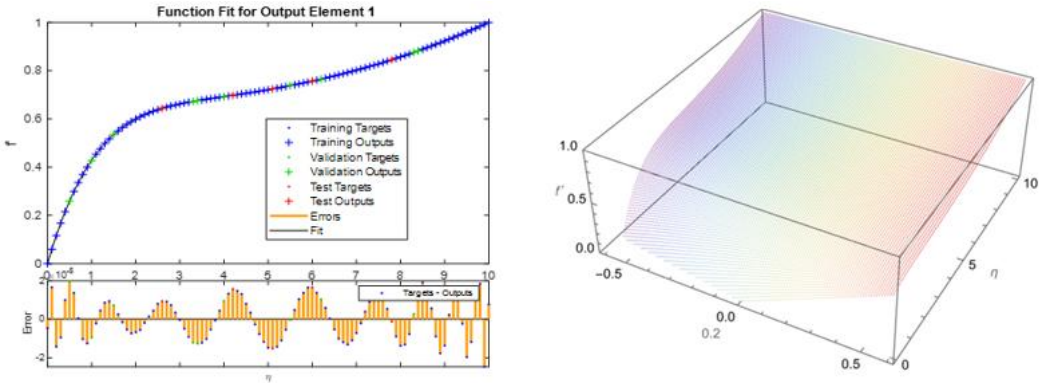

Figure 4. The validation results of $f'(\eta)$.

The results of validation $f'(\eta)$ (Figure 4) indicate the high congruency of numerical simulations and ANN algorithm outcomes, which proves the validity of the suggested model. The good correlation emphasizes the validity of the approach of the computations and the assumptions made. This steadiness strengthens the credibility of the model to be used in practice and it is therefore critical that scientific research should be validated carefully. The findings are also considerate of principles of accuracy and honesty, which makes the findings strong and replicable.

4 Comparison and validation

The results of the current study were carefully and in detail tested by comparing them with the results of previous studies. The results of the current study were compared with the results of [1] and [30] as well as the statistical model developed by [31]. The significance of the validation process is summarized in both Tables 4 and 5 of the manuscript and compared with $f''(0)$, by using different values of M and τ. In each case, values from the previous studies were very much aligned with the values produced from this study. This congruence, in particular, provides evidence regarding the reliability, accuracy, and robustness of the results derived from the current study and methodology. This validation against prior research establishes confidence in the validity of the proposed model, potential use in practice, and lends scientific support for EMHD nanofluid flow, generally. To assess the precision of the ANN architecture, we analyze and contrast the outcomes with the numerical method for both profiles (i.e., $f'(\eta)$ and $\theta(\eta)$) as presented in Tables 6 and 7.

Table 4. The comparison of $f''(0)$ results with the literature solution for different values of M.

M	Abbasbandy et al. [1]	Ibrahim Mahariq et al. [31]	ANN
0	1.232599	1.232598	1.23259985
2	2.346676	2.346679	2.34667925

Table 5. The comparison of $f''(0)$ results with the literature solution for different values of τ.

τ	Zainal et al. [30]	Ibrahim Mahariq et al. [31]	ANN
-0.5	1.4956698	1.4956697	1.495669704
0	1.2325877	1.2325881	1.232588102
0.5	0.7132950	0.7132949	0.713294903

Table 6. The comparison between numerical and ANN results for of $f'(\eta)$.

η	Numerical	ANN	Error
0.0	0.2	0.2	~ 0.0
2.0	0.65871701	0.658717025	$\sim 5.0 \times 10^{-9}$
4.0	0.7991481	0.799148095	$\sim 6.9 \times 10^{-8}$
6.0	1.00000013	1.0000000	$\sim 1.3 \times 10^{-7}$

Table 7. The comparison between numerical and ANN results for of $\theta(\eta)$.

η	Numerical	ANN	Error
0.0	1.0	1.0	~0.0
2.0	0.23322108	0.233221075	$\sim 1.4 \times 10^{-8}$
4.0	0.04997512	0.049975109	$\sim 1.7 \times 10^{-8}$
6.0	$2.62932611 \times 10^{-8}$	0.0000000	$\sim 2.6 \times 10^{-8}$

5 Results and discussion

The results presented here outline the complicated effects of the full range of governing parameters on the fundamental fluid flow and heat transfer characteristics of the system. In particular, this paper shows the effects on the following parameters: the velocity profile $f'(\eta)$, describing the movement of the fluid; the temperature profile $\theta(\eta)$, describing the heat distribution; the skin friction coefficient C_f, representing the frictional resistance at the surface; and finally the Nusselt number N_u, describing the convection. Each parameter has been appropriately studied to gain an understanding of its connections and effects on the boundary layer flow. This detailed presentation aims to understand the complexity of physical phenomena and provide valuable insights for possible applications and further research.

5.1. Effects on velocity profile f'(η)

Figures 5–12 provide a complete comparison of several critical parameters influencing the $f'(\eta)$ within the complex EMHD boundary layer flow of a ternary hybrid nanofluid. Considering a stretching parameter in Figure 5 is significant since $\lambda > 0$ represents a stretching surface that highly increases the velocity of the fluid modeling vigorous fluid motion. Conversely, the negative value of λ refers to a shrinking surface and it causes flow restriction due to the opposing forces within the boundary layer. Hence, we find it completely consistent with what is known in the fluid dynamics literature for these surfaces. In Figure 6, we illustrate the impact of the K_p describing an inverse relationship as it relates to increasing porosity with reduced fluid velocity. The reduced fluid velocity occurs due to an increase in drag resistance due to the porous medium which is an important consideration in the application of materials such as in filtration or geothermal energy extraction. Figure 7 focuses on the power-law index, which is particularly important in determining the velocity gradient close to the wall; larger values of *m* produce steeper profiles, indicating either an increased acceleration of the fluid or deceleration. This allows one to precisely control the properties of non-Newtonian fluid flow. In Figure 8, we focus on the magnetic parameter, M. Increasing M leads to consistently inhibiting the fluid velocity. This decrease in fluid velocity is due to the resistive Lorentz force, which opposes the motion of the fluid; this provides confirmation that magnetic fields can provide effective stabilization and control for flow in EMHD systems.

In Figure 9, we examine a resistive force, demonstrating how the Darcy-Forchheimer parameter produces significant reductions in $f'(\eta)$ due to the increased inertial drag. Consequently, this change in drag leads to a more flattened velocity profile illustrating that nonlinear resistance is far more dominant in the case of porous flows with high velocities. The effect of τ is shown in Figure 10. It clearly shows its role as a modifying influence on the boundary layer dynamics, though the physical interpretation requires further investigation. On the other hand, Figure 11 shows the positive influence

of the electric field E. Figure 11 illustrates the development of $f'(\eta)$ concerning the electrical field strengthened by electrokinetic driving forces. Consequently, this also shows a great potential for flow control via the synergistic interplay of electric and magnetic fields. Figure 12 is the final figure in this series, where the higher volume fractions correspond to lower velocities due to the higher viscosity of nanofluids. This indicates the critical need to carefully balance the thermal advantages of nanoparticles with their abilities to inhibit fluid flow.

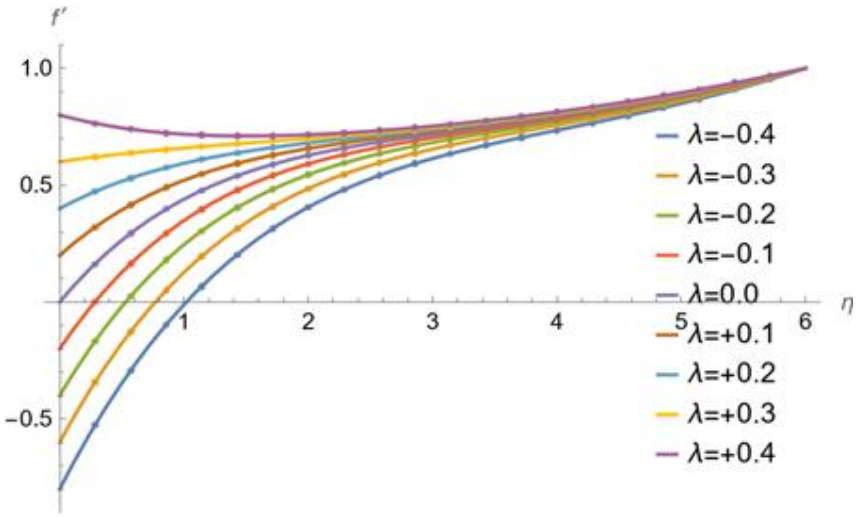

Figure 5. Effect of stretching/shrinking parameter on velocity profile.

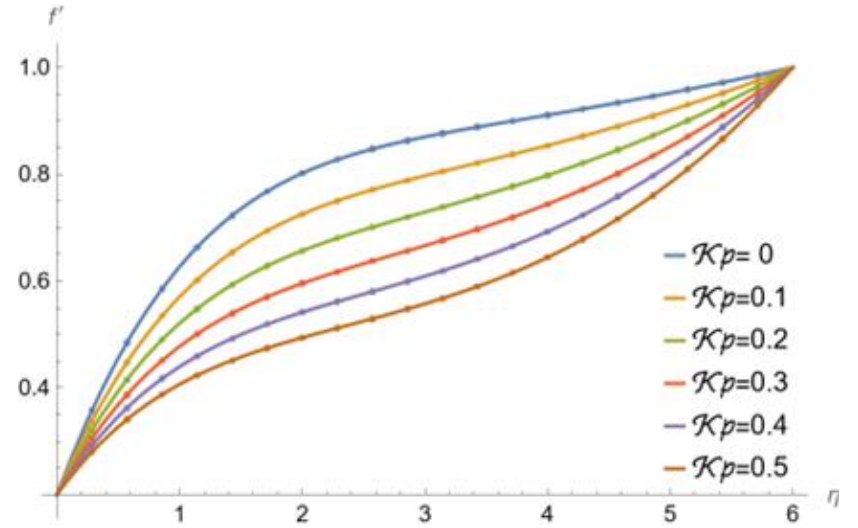

Figure 6. Effect of the porosity parameter on the velocity profile.

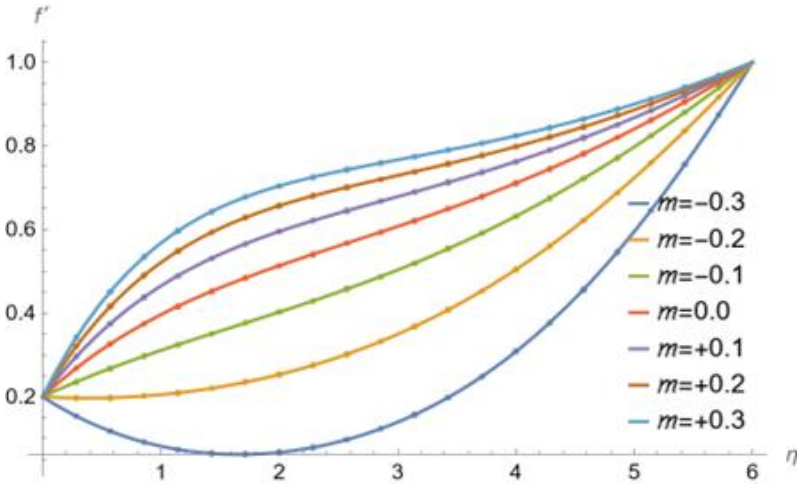

Figure 7. Impact of the power-law index on the velocity profile.

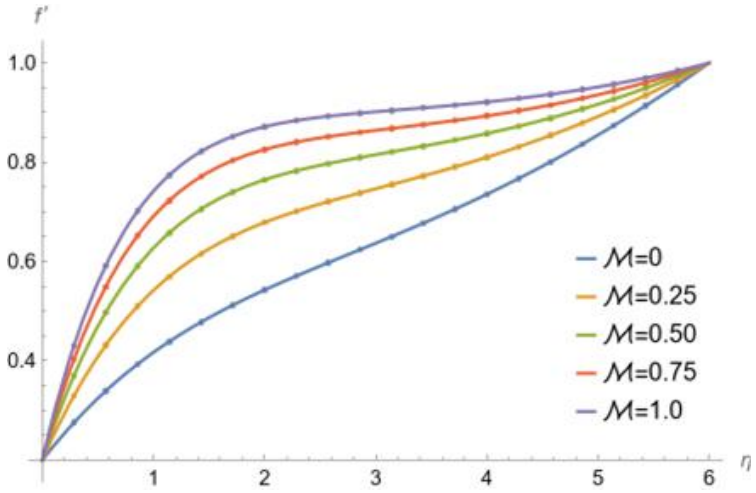

Figure 8. Effect of magnetic parameter on velocity profile.

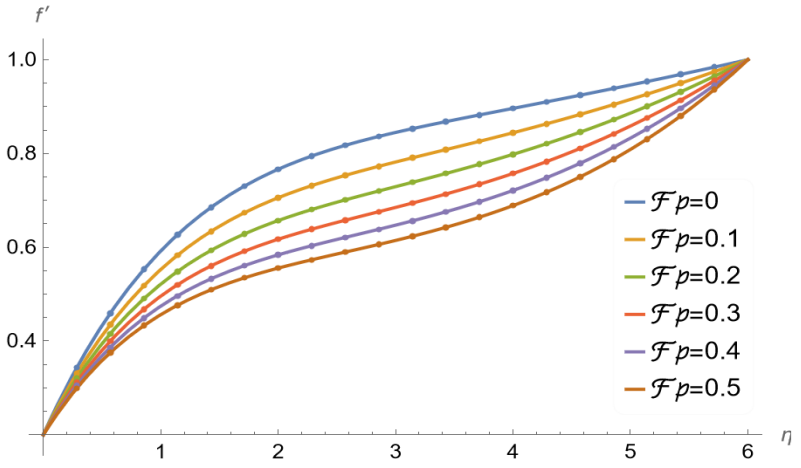

Figure 9. Effect of Darcy-Forchheimer parameter on velocity profile.

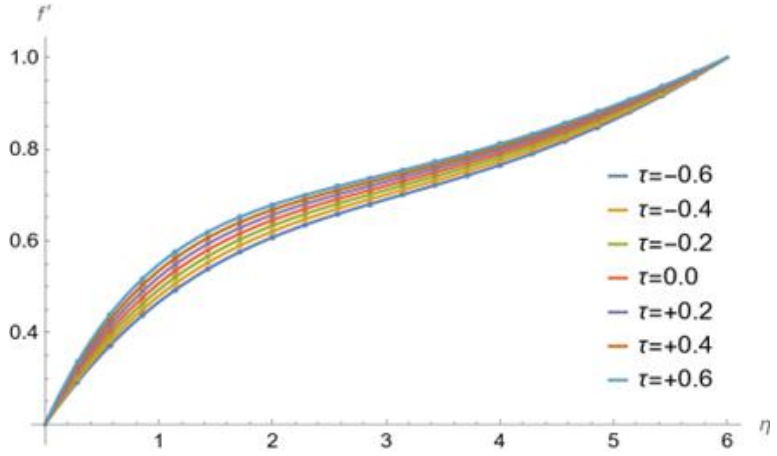

Figure 10. Effect of permeability parameter on velocity profile.

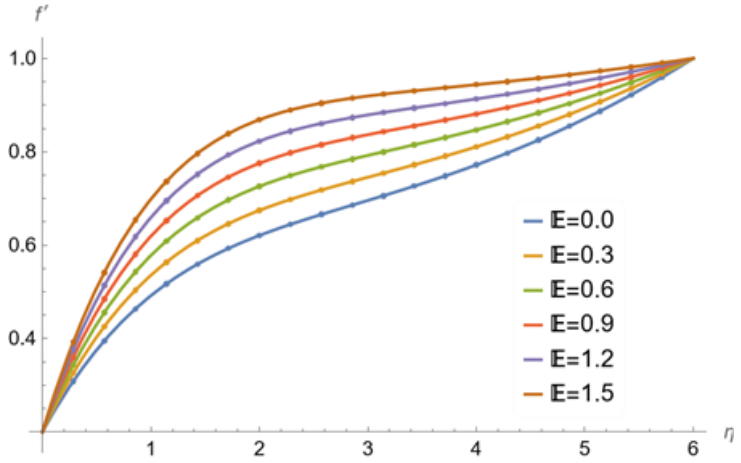

Figure 11. Effect of the electric field on the velocity profile.

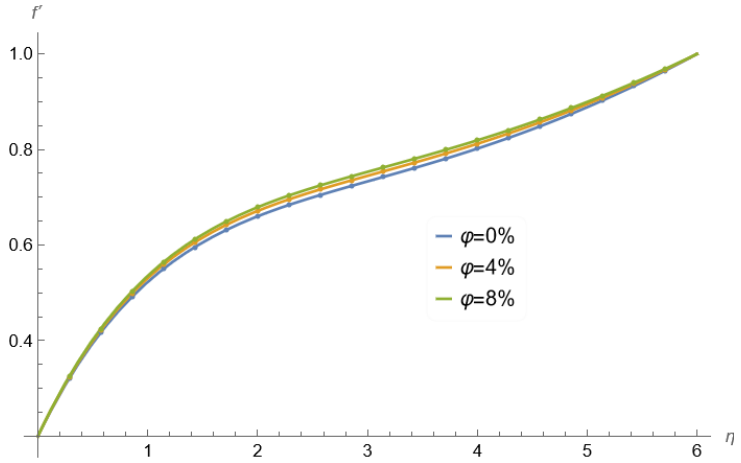

Figure 12. Influence of the volume fraction on the velocity profile.

5.2. Effects on temperature profile θ(η)

Figures 13–20 thoroughly demonstrate the complex influences of various parameters on the $\theta(\eta)$ in the EMHD boundary layer flow, which are critical to understanding the thermal behavior of the system. Figure 13 very clearly shows the thermal response to the stretching-shrinking parameter. For example, the shrinking surface ($\lambda < 0$) leads to an increase in the temperature of the fluid, while the stretching surface ($\lambda > 0$) leads to a reduction in the fluid temperature. This behavior is caused by changes in the boundary layer thickness and the heat dissipation, and is a well-known characteristic of thermal boundary layer analysis. Figure 14 provides details on the K_p parameter and shows that increasing porosity leads to increase the fluid temperature due to heat retention and reduced thermal dissipation (thus acting as an insulator), which is understandable in the context of porous media in heat exchangers. The power-law index is addressed in Figure 15. It has an indirect impact but it is a significant influence on thermal profiles. The large value of m often raises the temperature, because the fluid dynamics also change, which shows the link between the fluid rheology and thermal characteristics.

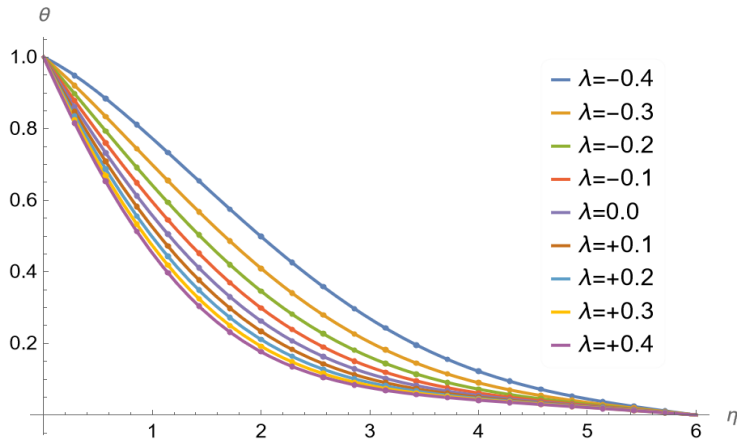

Figure 13. Temperature profile variation with the stretching/shrinking parameter.

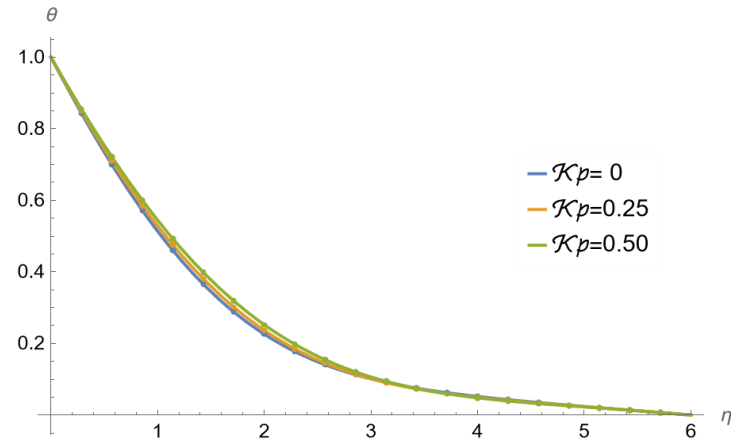

Figure 14. Effect of Porosity parameter on temperature profile.

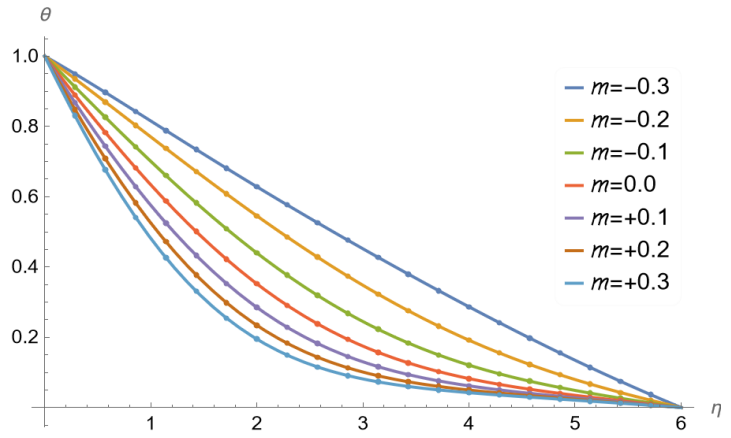

Figure 15. Effect of the power-law index on the temperature profile.

Figure 16 considers the magnetic parameter and demonstrates that an increase in M leads to a rise in temperature due to Joule heating. There very much exists a very strong need to find a balance between magnetic control and thermal management in EMHD systems. Conversely, Figure 17 demonstrates the beneficial effect seen in the radiation parameter, as increases in Rd lead to a sharp decrease in the temperature by enhancing heat dissipation. It is a useful property in monitoring the radiation potential and radiation's cooling potential, which is vital for high-temperature industrial processes. Figure 18 suggests a thermal role for porosity parameter τ, but future work is needed to clarify τ. It is a thermal influence on the boundary layer heat transfer and indicates shear-thermal interactions. Figure 19 looks at the electric field. It is shows that increasing E raises the temperature through additional Joule heating, emphasizing the dual role of EMHD in flow and heat control as will as the need to find a critical balance in device design. Figure 20 is a final figure with a short discussion on nanoparticle φ that raises the temperature by enhancing thermal conductivity, but this benefit must be balanced against the potential flow impediment due to increased viscosity. Collectively, these figures demonstrate how surface dynamics, porous media characteristics, fluid rheology, electromagnetic forces, and radiative effects are all interlinked to govern the thermal profile, providing sufficient detail to make routing of the design and optimize of advanced thermal management systems and EMHD applications.

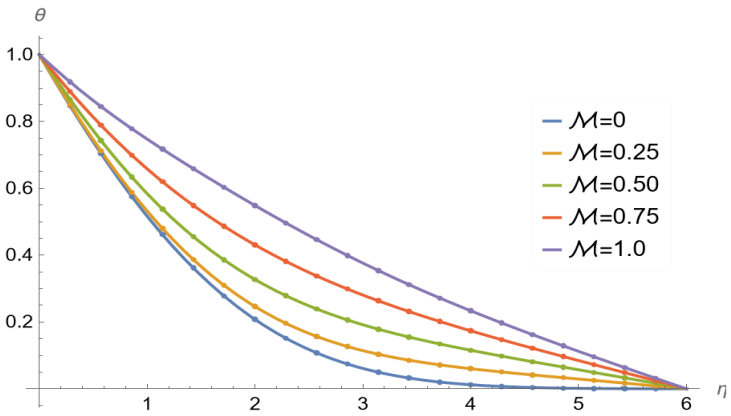

Figure 16. Effect of magnetic parameter on temperature profile.

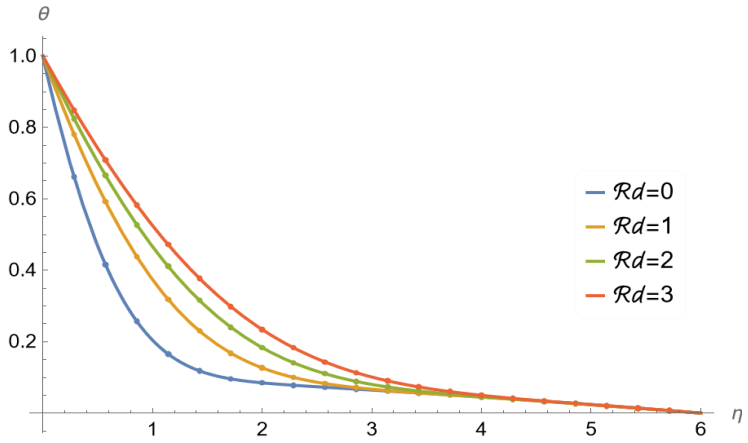

Figure 17. Effect of radiation parameter on temperature profile

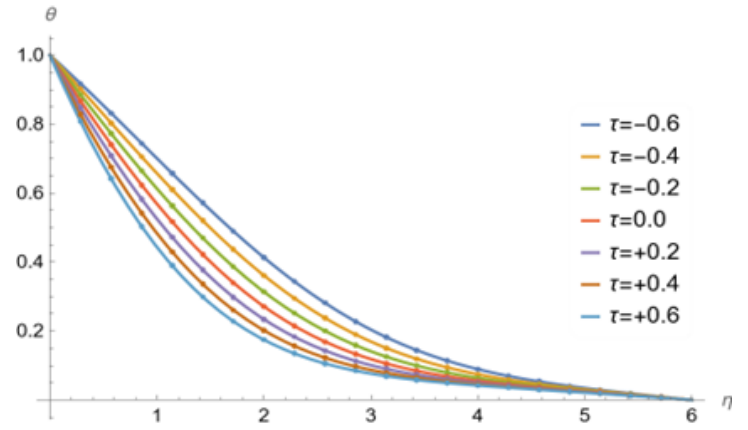

Figure 18. Temperature profile variation with the porosity parameter.

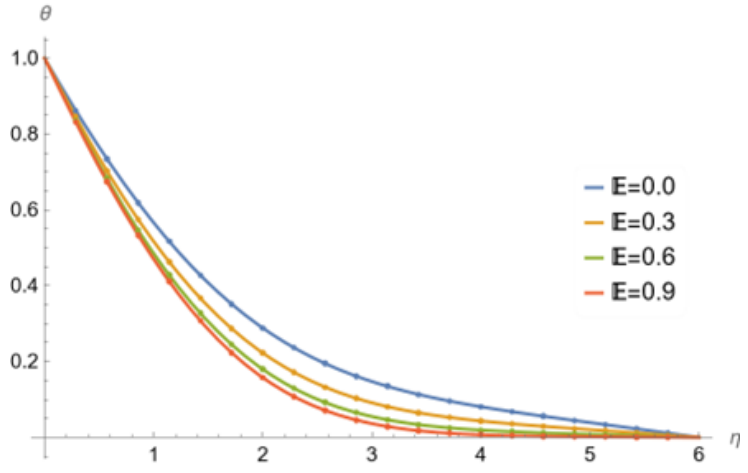

Figure 19. Effect of the electric field on the temperature profile.

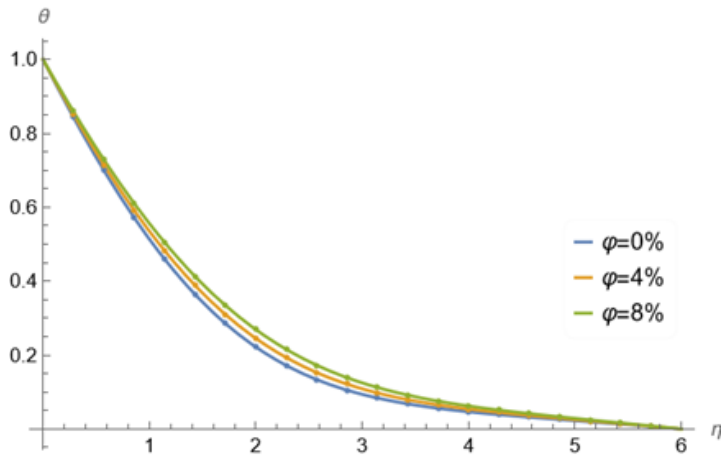

Figure 20. Effect of volume fraction on temperature profile.

5.3. Combined effects on skin friction and the Nusselt number

Collectively, Figures 21–24 present a complete, detailed discussion of how different parameters interact to impact two critical engineering coefficients, which are the skin friction coefficient and the Nusselt number. Both of them provide key information about the fluid flow and heat transfer characteristics of the system. Specifically, Figure 21 details a combination effect of porosity and the stretching-shrinking parameter on Cf. The relationship is clearly understood in that skin friction increases significantly with both increasing porosity, as more drag accompanies the resistance generated in the porous medium, and with shrinking surfaces ($\lambda < 0$), which inherently generate elevated shear stress at the wall. This interaction is critical for applications where minimizing drag is crucial, such as in microfluidic devices and lubrication systems, and the complicated impact between porous drag and surface dynamics. Subsequently, Figure 22 examines the combined impact of K_p and λ on the Nusselt number, which indicates the rate of heat transfer. The interesting opposing trends are shown in the analysis, as N_u decreases with increasing K_p, indicating that porosity acts as an insulator, inhibiting efficient heat transfer. It grows with stretching surfaces ($\lambda > 0$), as these stretching surfaces enhance convective heat transfer by reducing the thermal boundary layer thickness. The opposing trend requires a careful balance between the insulating properties of porosity and the heat transfer enhancement from stretching. It is very important for improving the thermal performance of heat exchangers and similar thermal management devices. The impact of the Darcy-Forchheimer parameter and the electric field on Cf is shown in Figure 23. The results show that both inertial drag Fr, stemming from the porous medium, and the electric field, acting on the fluid, increase skin friction. Ultimately, their combination causes a dramatic increase in energy losses within EMHD flows, which can have important implications for system efficiency. This is an important figure because it illustrates the inherent trade-offs in controlling a flow; to improve certain flow properties may inadvertently lead to increased frictional resistance. Finally, Figure 24 adds to this exploration by exhibiting the combined effects of Fr and E on the Nusselt number. The opposite effect is observed, as N_u increases with increasing E which indicates that electric fields improve heat transfer, and is likely through increased motion in the fluid with savings in electro-convective effects, while N_u decreases with increasing Fr. This decrease indicates that inertial drag resists heat transfer and it is likely through disrupting the thermal boundary layer or decreasing the effectiveness of fluid mixing. Therefore, careful

consideration of these two parameters is important for the thermal performance of EMHD systems. These four figures represent extremely valuable contributions to understanding the complex interplay between fluid dynamics, heat transfer, and electromagnetic forces. These together support the development of more efficient EMHD heat transfer models for a range of engineering applications. Furthermore, these figures highlight the need for a holistic approach to system optimization.

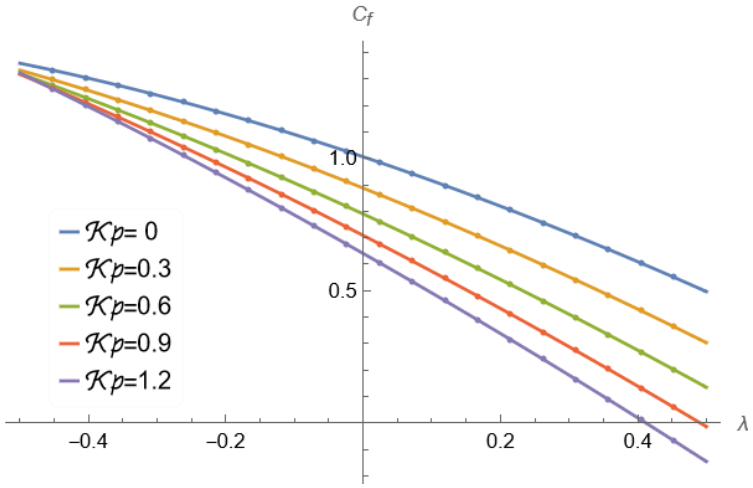

Figure 21. Combined effects of porosity and stretching/shrinking on the skin friction coefficient.

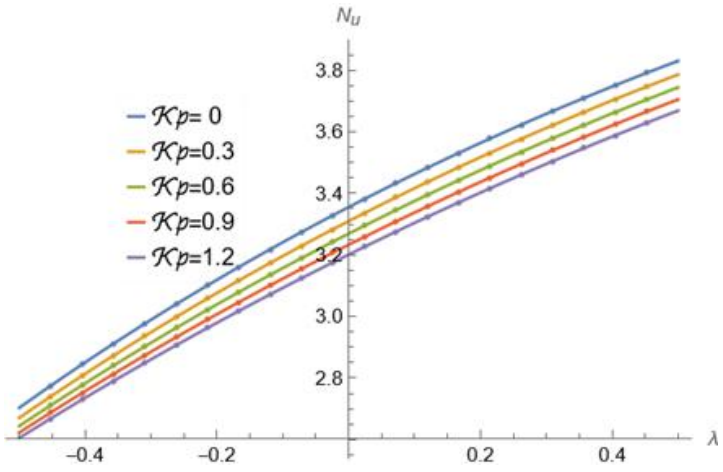

Figure 22. Combined effects of porosity and stretching/shrinking on the Nusselt number.

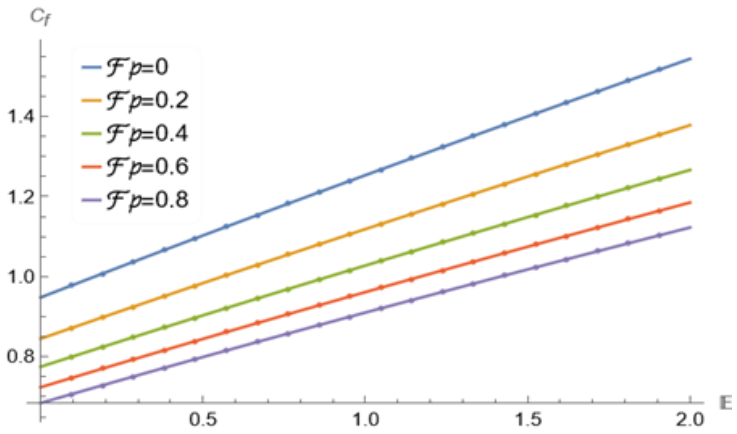

Figure 23. Combined effects of the Darcy-Forchheimer parameter and electric field on the skin friction coefficient.

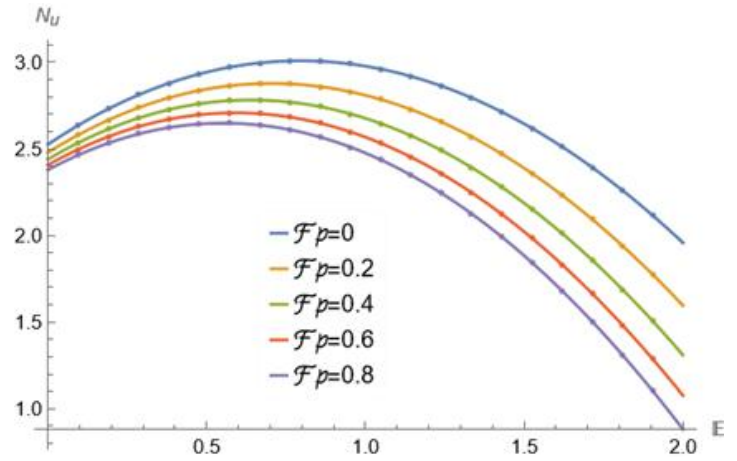

Figure 24. Combined effects of the Darcy-Forchheimer parameter and electric field on the Nusselt number.

6. Conclusions

The present study provides a comprehensive investigation into the complex electro-magnetohydrodynamic boundary layer flow of a ternary hybrid nanofluid past stretching-shrinking and permeable surfaces, where the Darcy-Forchheimer law is considered with thermal radiation effects. The study successfully applied an artificial neural network as an intelligent numerical technique to solve the governing equations, demonstrating its accuracy and robustness. The study can be applied to several conclusions, including:

- The intelligent numerical approach of an ANN was very efficient and reliable, where its prediction was strongly aligned with the numerical simulations and existing literature, which proves its applicability in such complex fluid dynamics problems.
- The stretching surfaces ($\lambda > 0$) and electric fields dominate in organizing to enhance the fluid velocity, whereas an increased porosity parameter, magnetic fields, and Darcy-Forchheimer effects were dominant in slowing the flow as a consequence of the increased drag or resistive forces.

- For shrinking surfaces ($\lambda < 0$), increased porosity, magnetic fields, and electric fields dominate for increasing temperatures, which was often due to reduced thermal dissipation or Joule heating. Conversely, stretching surfaces ($\lambda > 0$) and thermal radiation promoted cooling.
- With higher concentrations of nanoparticles, a reduction in fluid velocity due to increased fluid viscosity and increases in temperature due to increases in thermal conductivity highlight a critical balance for optimal system design.
- Skin friction also increased using large porosity, shrinking surfaces ($\lambda < 0$), Darcy-Forchheimer effects, and electric fields, which indicates increased energy losses.
- The Nusselt number as a gauge of heat transfer performance is typically increased using stretching surfaces ($\lambda > 0$) and electric fields, and typically decreased by increasing porosity and Darcy-Forchheimer effects.

Author contributions

Abdulaziz H. Alharbi: Writing–original draft, methodology, investigation, conceptualization, software, supervision, project administration; El Hadi Boussaha: Writing–original draft, conceptualization, software, methodology; Ali M. Alhartomi: Methodology, funding acquisition, investigation, writing–review and editing; Hicham Salhi: Conceptualization, methodology, writing–review and editing; Raed Alrdadi: Writing–original draft, investigation, methodology; Mohamed Kezzar: Writing–original draft, methodology, investigation, conceptualization, software; Mohamed Rafik Sari: Methodology, investigation, conceptualization, writing–review and editing. All authors have read and agreed to the published version of the manuscript.

Use of Generative-AI tools declaration

The authors declare they have not used Artificial Intelligence (AI) tools in the creation of this article.

Acknowledgments

The authors extend their appreciation to Umm Al-Qura University, Saudi Arabia, for funding this research work through grant number 25UQU4340278GSSR01.

Funding

This research work was funded by Umm Al-Qura University, Saudi Arabia, under grant number 25UQU4340278GSSR01.

Conflict of interest

The authors claim that they have no conflicts of interest in publishing this work.

References

1. S. Abbasbandy, T. Hayat, A. Alsaedi, M. M. Rashidi, Numerical and analytical solutions for Falkner-Skan flow of MHD Oldroyd-B fluid, *Int. J. Numer. Method. H.*, **24** (2014), 390–401. https://doi.org/10.1108/HFF-05-2012-0096
2. T. Hayat, A Shafiq, A Alsaedi, S Asghar, Effect of inclined magnetic field in flow of third grade fluid with variable thermal conductivity, *AIP Adv.*, **5** (2015), 087108. https://doi.org/10.1063/1.4928321
3. M. R. Eid, K. L. Mahny, Unsteady MHD heat and mass transfer of a non-Newtonian nanofluid flow of a two-phase model over a permeable stretching wall with heat generation/absorption, *Adv Powder Technol.*, **28** (2017), 3063–3073. https://doi.org/10.1016/j.apt.2017.09.021
4. S. Gherieb, M. Kezzar, A. Nehal, M. R. Sari,A new improved generalized decomposition method (improved-GDM) for hydromagnetic boundary layer flow, *Int. J. Numer. Method. H.*, **30** (2020), 4607–4628. https://doi.org/10.1108/HFF-08-2019-0655
5. L. Ali, B. Ali, K. K. Asogwa, R. Apsari, Transient rotating three-dimensional flow of micropolar fluid induced by Riga plate: finite element approach, *Numer. Heat Tr. A-Appl.*, **85** (2024), 1889–1902. https://doi.org/10.1080/10407782.2023.2212861
6. L. Ali, R. Apsari, A. Abbas, P. Tak, Entropy generation on the dynamics of volume fraction of nano-particles and coriolis force impacts on mixed convective nanofluid flow with significant magnetic effect, *Numer. Heat Tr. A-Appl.*, **86** (2025), 8509–8524. https://doi.org/10.1080/10407782.2024.2360652
7. M. Sheikholeslami, D. D. Ganji, Nanofluid convective heat transfer using semi analytical and numerical approaches: A review, *J. Taiwan Inst. Chem. E.*, **65** (2016), 43–77. https://doi.org/10.1016/j.jtice.2016.05.014
8. O. Mahian, A. Kianifar, S. A. Kalogirou, I. Pop, S. Wongwises, A review of the applications of nanofluids in solar energy, *Int. J. Heat Mass Tran.*, **57** (2013), 582–594. https://doi.org/10.1016/j.ijheatmasstransfer.2012.10.037
9. M. M. Rashidi, N. V. Ganesh, A. K. A. Hakeem, B. Ganga, Buoyancy effect on MHD flow of nanofluid over a stretching sheet in the presence of thermal radiation, *J. Mol. Liq.*, **198** (2014), 234–238. https://doi.org/10.1016/j.molliq.2014.06.037
10. P. Z. Forchheimer, Wasserbewegung durch boden, *Zeitschrift des Vereines Deutscher Ingenieure*, **45** (1901), 1781–1788.
11. M. A. Seddeek, Influence of viscous dissipation and thermophoresis on Darcy-Forchheimer mixed convection in a fluid saturated porous media, *J. Colloid Interf. Sci.*, **293** (2006), 137–142. https://doi.org/10.1016/j.jcis.2005.06.039
12. P. A. Davidson, *Introduction to magnetohydrodynamics*, 2 Eds., Cambridge: Cambridge University Press, 2016. https://doi.org/10.1017/9781316672853
13. L. Ali, P. Kumar, H. Poonia, S. Areekara, R. Apsari, The significant role of Darcy-Forchheimer and thermal radiation on Casson fluid flow subject to stretching surface: A case study of dusty fluid, *Mod. Phys. Lett. B*, **38** (2024), 2350215. https://doi.org/10.1142/S0217984923502159
14. G. W. Sutton, A. Sherman, *Engineering magnetohydrodynamics*, New York: Dover Publications, 2006.
15. R. Moreau, *Magnetohydrodynamics*, Dordrecht: Springer, 2013.

16. R. R. Sahoo, V. Kumar, Development of a new correlation to determine the viscosity of ternary hybrid nanofluid, *Int. Commun. Heat Mass*, **111** (2020), 104451. https://doi.org/10.1016/j.icheatmasstransfer.2019.104451
17. H. Adun, D. Kavaz, M. Dagbasi, Review of ternary hybrid nanofluid: Synthesis, stability, thermophysical properties, heat transfer applications, and environmental effects, *J. Clean. Prod.*, **328** (2021), 129525. https://doi.org/10.1016/j.jclepro.2021.129525
18. S. M. Mousavi, F. Esmaeilzadeh, X. P. Wang, A detailed investigation on the thermo-physical and rheological behavior of MgO/TiO_2/water-ethylene glycol hybrid nanofluid, *J. Mol. Liq.*, **282** (2019), 323–339. https://doi.org/10.1016/j.molliq.2019.02.100
19. Z. H. Xuan, Y. L. Zhai, M. Y. Ma, Y. H. Li, H. Wang, Thermo-economic performance and sensitivity analysis of ternary hybrid nanofluids, *J. Mol. Liq.*, **323** (2021), 114889. https://doi.org/10.1016/j.molliq.2020.114889
20. T. Hayat, M. Waqas, S. A. Shehzad, A. Alsaedi, Stretched flow of Carreau nanofluid with convective boundary condition, *Pramana*, **86** (2016), 3–17. https://doi.org/10.1007/s12043-015-1137-y
21. W. A. Khan, I. Pop, Boundary-layer flow of a nanofluid past a stretching sheet, *Int. J. Heat Mass Tran.*, **53** (2010), 2477–2483. https://doi.org/10.1016/j.ijheatmasstransfer.2010.01.032
22. A. Wakif, M. Zaydan, R. Sehaqui, Aspects of EMHD boundary layer flows for alumina-water nanofluidic mixtures in a porous medium, *J. Umm Al-Qura Univ. Appll. Sci.*, (2024). https://doi.org/10.1007/s43994-024-00174-6
23. P. Mushahary, S. Enamul, S. Ontela, Thermal analysis of mixed convective electro-osmotic thermally radiative EMHD flow of couple stress hybrid nanofluid in a vertical porous channel, *Chinese J. Phys.*, **97** (2025), 385–410. https://doi.org/10.1016/j.cjph.2025.03.011
24. I. E. Lagaris, A. Likas, D. I. Fotiadis, Artificial neural networks for solving ordinary and partial differential equations, *IEEE T. Neural Networ.*, **9** (1998), 987–1000. https://doi.org/10.1109/72.712178
25. M. Raissi, P. Perdikaris, G. E. Karniadakis, Physics-informed neural networks: A deep learning framework for solving forward and inverse problems involving nonlinear partial differential equations, *J. Comput. Phys.*, **378** (2019), 686–707. https://doi.org/10.1016/j.jcp.2018.10.045
26. M. W. M. G. Dissanayake, N. Phan-Thien, Neural-network-based approximations for solving partial differential equations, *Commun. Numer. Meth. En.*, **10** (1994), 195–201. https://doi.org/10.1002/cnm.1640100303
27. K. Hornik, M. Stinchcombe, H. White, Multilayer feedforward networks are universal approximators, *Neural Networks*, **2** (1989), 359–366. https://doi.org/10.1016/0893-6080(89)90020-8
28. M. Bahiraei, S. Heshmatian, H. Moayedi, Artificial intelligence in the field of nanofluids: A review on applications and potential future directions, *Powder Technol.*, **353** (2019), 276–301. https://doi.org/10.1016/j.powtec.2019.05.034
29. F. Zia, J. Iqbal, N. Naheed, M. M. Alam, AI-powered analysis of thermally magnetized EMHD Casson hybrid nanofluid, *Case Stud. Therm. Eng.*, **74** (2025), 106812. https://doi.org/10.1016/j.csite.2025.106812
30. N. A. Zainal , R. Nazar, K. Naganthran, I. Pop, Unsteady MHD hybrid nanofluid flow towards a horizontal cylinder, *Int. Commun. Heat Mass*, **134** (2022), 106020. https://doi.org/10.1016/j.icheatmasstransfer.2022.106020

31. I. Mahariq, R. Saadeh, F. L. Rashid, A. Qazza, H. A. E. W. Khalifa, M. Kezzar, et al., Role of ternary hybrid nanoparticle and EMHD on boundary layer flow with stretching-shrinking plate: Optimization analyses using RMS, *Results Phys.*, **74** (2025), 108315. https://doi.org/10.1016/j.rinp.2025.108315

Appendix A

The thermophysical properties of THNF are presented in both Tables A.1 and A.2.

Table A.1. Physical properties of nanofluids and THNF.

Character	Formula
Dynamic viscosity	$\mu_{thnf} = \mu_f(1-\varphi_1)^{-2.5}(1-\varphi_2)^{-2.5}(1-\varphi_3)^{-2.5}$
Density	$\rho_{thnf} = (1-\varphi_1)\{(1-\varphi_2)[(1-\varphi_3)\rho_f + \varphi_3\rho_{s3}] + \varphi_2\rho_{s2}\} + \varphi_1\rho_{p1}$
Specific heat	$(\rho C_p)_{thnf} = (1-\varphi_1)\{(1-\varphi_2)[(1-\varphi_3)(\rho C_p)_f + \varphi_3(\rho C_p)_{s3}] + \varphi_2(\rho C_p)_{s2}\} + \varphi_1(\rho C_p)_{s1}$
Electrical conductivity	$\frac{\sigma_{Thnf}}{\sigma_{hnf}} = \frac{\sigma_{s1} + 2\sigma_{hnf} - 2\varphi_1(\sigma_{hnf} - \sigma_{s1})}{\sigma_{s1} + 2\sigma_{hnf} - \varphi_1(\sigma_{hnf} - \sigma_{s1})}$, $\frac{\sigma_{hnf}}{\sigma_{nf}} = \frac{\sigma_{s2} + 2\sigma_{nf} - 2\varphi_2(\sigma_{nf} - \sigma_{s2})}{\sigma_{s2} + 2\sigma_{nf} - \varphi_2(\sigma_{nf} - \sigma_{s2})}$, $\frac{\sigma_{nf}}{\sigma_f} = \frac{\sigma_{s3} + 2\sigma_f - 2\varphi_3(\sigma_f - \sigma_{s3})}{\sigma_{s3} + 2\sigma_f - \varphi_3(\sigma_f - \sigma_{s3})}$.
Thermal conductivity	$\frac{k_{Thnf}}{k_{hnf}} = \frac{k_{s1} + 2k_{hnf} - 2\varphi_1(k_{hnf} - k_{s1})}{k_{s1} + 2k_{hnf} - \varphi_1(k_{hnf} - k_{s1})}$, $\frac{k_{hnf}}{k_{nf}} = \frac{k_{s2} + 2k_{nf} - 2\varphi_2(k_{nf} - k_{s2})}{k_{p2} + 2k_{nf} - \varphi_2(k_{nf} - k_{s2})}$, $\frac{k_{nf}}{k_f} = \frac{k_{s3} + 2k_f - 2\varphi_3(k_f - k_{s3})}{k_{s3} + 2k_f - \varphi_3(k_f - k_{s3})}$.

Table A.2. Thermophysical properties of water and nanoparticles.

Physical properties	ρ (kg/m^3)	C_p(J/kg.°K)	k(W/m.°K)	σ(S/m)
Water	997.1	4179	0.613	0.05
Ti6Al4V → $\blacksquare_{s1}$	4420	0.56	7.2	5.8×10^5
ZnO → $\blacksquare_{s2}$	5600	544	19	10^{-2}
Fe_2O_3 → $\blacksquare_{s3}$	5200	670	9.7	0.74×10^6